Spectroscopic Analysis of *Candida* Species, Viability, and Antifungal Drug Effects With a Microwave Flow Cytometer

Neelima Dahal, Jeffrey A. Osterberg, Benjamin Braun, Tom P. Caldwell, Ralu Divan, Sarah W. Harcum, and Pingshan Wang, *Senior Member, IEEE*

***Abstract*—New methods to rapidly detect and identify *Candida* cells in patients' blood is needed for proper candidemia treatment. In this work, a tunable microwave interferometer was used to measure single *Candida* cells of *C. albicans*, *C. tropicalis*, *C. parapsilosis*, and *C. krusei* at multiple frequencies between 0.265 GHz and 7.76 GHz. The obtained permittivity values $\Delta\varepsilon'$ and $\Delta\varepsilon''$ of non-budding *Candida* were colinear with cell volumes and had a coefficient that depends on measurement frequency, cell species and viability. Viable and non-viable cells had significant permittivity differences at lower frequency spectrum, but with substantial overlap at 7.76 GHz. For single non-budding cells, measurements at 1.32 GHz and 1.85 GHz enabled a minimum 0.875 classification accuracy with quadratic discriminate analysis (QDA). However, cell budding induced significant microwave property overlaps. Further work is needed to achieve better cell species discrimination. Additionally, it was determined that treating these yeast cells with Caspofungin (CSP) diacetate in dimethyl sulfoxide (DMSO) for 10 minutes significantly altered cell microwave properties. This change was likely due to damaged cell wall and membranes, and the level of change was *Candida* species dependent. Therefore, broadband microwave measurement is a promising new approach for physicians to provide personalized candidemia therapy.**

***Index Terms*—Microwave sensing, complex permittivity, Candida, antifungal drug resistance, cytometry.**

I. Introduction

CANDIDA species are the fourth most common nosocomial bloodstream pathogens [1]. *C. albicans*, *C. tropicalis*, *C. parapsilosis*, *C. glabrata*, and *C. krusei* account for more than 95% of candidemia cases of hospitalized patients. The average annual incidence of candidemia is approximately 9 per 100000 population in the US [2] with 19-24% attributable mortality rate and $40000/case treatment cost [3]. A 12-hour delay of proper antifungal therapy can increase the mortality rate by up to 20% [4]. This healthcare problem is growing due to the increasing at-risk population that can now survive other diseases owing to medical technology advancements and the spreading antifungal-drug-resistant yeast species, such as *C. auris* and *C. glabrata*. The antifungal drug resistance challenge is largely driven by the excess use of antibiotic and antifungal drugs. Thus, timely and comprehensive information of *Candida* species and yeast cell antifungal susceptibility test (AFST) is critical for physicians to make informed decisions on candidemia treatment, including the selection of an optimal antifungal agent and the termination of unnecessary antifungal drug usage.

Nevertheless, no clinical signs or symptoms are specific for candidemia [5] and 50% of the patients have less than 1 cfu/mL *Candida* in their blood. Currently, cell culture and microscopic observation remain the standard methods for *Candida* detection, identification, and AFST. But these methods can take days to obtain results [23]. Among various non-culture methods, polymerase chain reaction (PCR) based molecular methods, next generation sequencing (NGS), and matrix-assisted laser desorption/ionization-time of flight mass spectroscopy (MALDI-TOF MS) are both rapid and accurate in detecting *Candida* presence in patient blood sample; however not as accurate at identifying yeast species or predicting cell AFST. For instance, it takes approximately 4 hours for T2Candida to detect the 5 species of *Candida* in patients' blood [6] without prior blood culture or nucleic acid extractions. Though *C. albicans*/*C. tropicalis* and *C. glabrata* complex/*C. krusei* are identified as two groups [1], similar AFST profiles in each group help T2Candida in clinical applications. Yet, the method is expensive and lacks AFST option. The other methods are often limited by sample preparation, technology complexity, or high cost. As a result, these methods are difficult to use in point-of-care (POC) settings or managing potential candidemia outbreaks [7] or preventing wide-scale candidemia spread [8]. Therefore, new methods are needed for rapid *Candida* detection, identification, and AFST.

Recent development of dielectric spectroscopy (DS) for single cell analysis has shown that DS is promising to help address candidemia diagnosis needs. At MHz and lower frequencies,

Manuscript received 28 March 2022; revised 25 May 2022; accepted 15 June 2022. Date of publication 14 September 2022; date of current version 24 November 2022. This work was supported in part by the US Army Office of Research under Grant W911NF2110145, in part by the NSF under Grant 1711463, in part by the Center for Nanoscale Materials, an Office of Science user Facility, and in part by the U.S. Department of Energy, Office of Science, Office of Basic Energy Sciences under Grant DE-AC02-06CH11357. *(Corresponding author: Pingshan Wang.)*

Neelima Dahal, Jeffrey A. Osterberg, and Pingshan Wang are with the Holcomb Department of Electrical and Computer Engineering, Clemson University, Clemson, SC 29634 USA (e-mail: ndahal@clemson.edu; josterb@clemson.edu; pwang@clemson.edu).

Benjamin Braun is with the School of Computing, Clemson University, Clemson, SC 29634 USA (e-mail: braun4@clemson.edu).

Tom P. Caldwell and Sarah W. Harcum are with the Department of Bioengineering, Clemson University, Clemson, SC 29634 USA (e-mail: clemsonscooby@gmail.com; harcum@clemson.edu).

Ralu Divan is with the Argonne National Laboratory, Center for Nanoscale Materials, Lemont, IL 60439 USA (e-mail: divan@anl.gov).

Digital Object Identifier 10.1109/JERM.2022.3201698

label-free impedance measurement of single white blood cells has shown that cell sub-populations have significantly different electrical properties (i.e., opacity) for cell differentiation with 95% correlation against commercial (optical/Coulter) blood analysis equipment [9]. Viable and non-viable cells exhibit different impedance values [14]. The measured differences likely come from cell size and membrane property differences since low frequency probing fields are often blocked by electrical double layers on membrane surfaces [10]. Cell shape [11] and orientation [12], [13] also affect cell impedance properties. At higher frequencies, probing fields can penetrate through cell walls, thus, interact with cell organelles and cytoplasm [10]. So, more cell information is expected compared to low frequency impedance measurement. A microwave-based sensor was used in [15] to discriminate *S. cerevisiae* and *S. pastorianus* [15], which have similar shapes and sizes and traditionally need molecular methods to differentiate. The lowest uncertainty if using single-frequency measurements were observed at 2.38 GHz and 265 MHz with cross-validation errors of 27% and 15%, respectively. Therefore, it is of great interest to investigate if microwave measurement can differentiate *Candida* species and detect cell antifungal drug effects.

In this work, we characterized four species of *Candida* under flow conditions using a simple microwave flow cytometer at multiple frequencies. We showed the microwave detection of *Candida* antifungal drug effects. These results indicate that broadband microwave techniques offer a potential and new POC method for rapid candidemia diagnosis.

II. Material and Methods

A. Candida and Sample Preparation

The four species of freeze-dried *Candida* i.e., *C. albicans* (ATCC No. 18804), *C. tropicalis* (ATCC No. 13803), *C. parapsilosis* (ATCC No. 90018), and *C. krusei* (ATCC No. 14243), were purchased from the American Type Culture Collection (www.atcc.org). Each yeast species was cultured in 50 mL YPD (Yeast Extract–Peptone–Dextrose) in an orbital shaker at 250 rpm and 30 °C for approximately 4 h. Freezer stocks were then prepared by mixing 700 μL of this incubated culture in 300 μL of 50% glycerol each and stored at -80 °C. YPD was prepared as described in [22] and contained 10 g/L yeast extract, 20 g/L peptone, and 20 g/L dextrose. Prior to microwave measurement, 1 mL of freezer stock was cultured in 50 mL sterile YPD medium in an orbital shaker at 250 rpm and 30 °C overnight (approximately 18 h).

Cell concentration was determined by measuring the optical density (OD) of a 1 mL diluted sample (950 μL DI water and 50 μL cell culture) at 600 nm (Spectronic 30 Genesys, ThermoFisher). The OD600 was zeroed with 950 μL DI water. The yeast cultures were then transferred into 1.5 mL tubes for microwave testing.

Non-viable yeast cells were prepared by heat shocking viable cells at 90 °C for 1 minute. Trypan blue was used to verify cell viability with a hemocytometer. Approximately 100% of the cells were viable prior to heat-shock, and all were non-viable following heat-shock. Both viable and non-viable yeast cells were stored at room temperature during microwave testing.

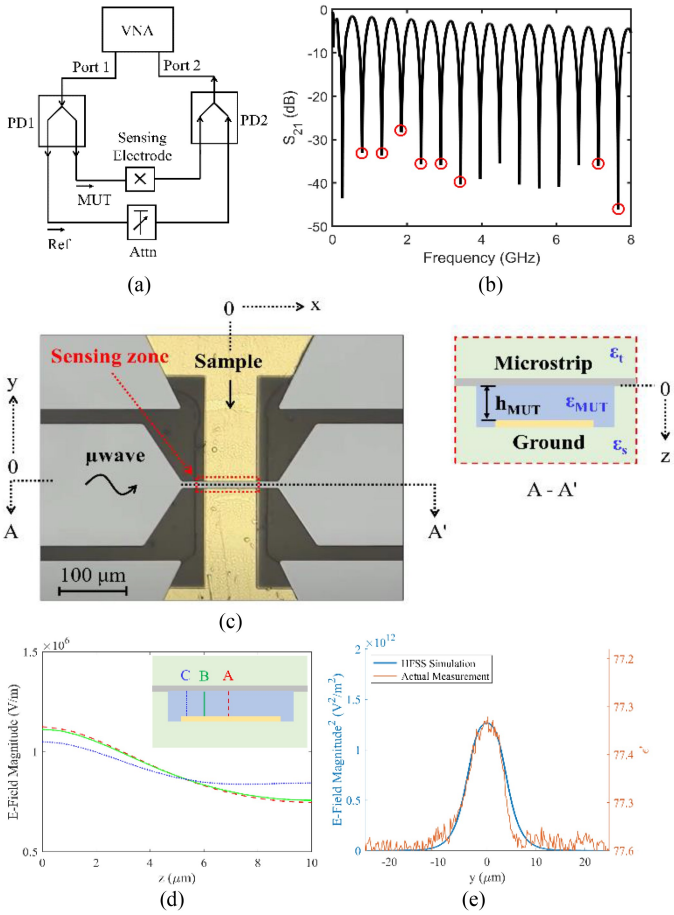

Fig. 1. (a) A schematic of the microwave flow cytometer measurement system, which consists of a vector network analyzer (VNA) and a tunable interferometer. Sample injection and control is not shown. (b) Typical broadband S21 magnitude (measured). The notch frequencies are measurement frequencies, such as those labeled with red circles. (c) A picture of the microwave sensing electrode, which is a microstrip line. Zoom-in: A cross section of the electrode on two 1 mm thick glass substrates. The sensing zone showing h_{MUT} = 10 μm. (d) Simulated field distributions along lines A (0, 0, z), B (-28 μm,0, z), and C (-45.5 μm, 0, z) at f = 1.0 GHz with 1 W microwave power. For cell measurement in Section III, the VNA power was set at 0 dBm. Considering power transmission in (b), it's estimated that much less than 0.1 dBm is absorbed by liquid sample which is flowing. As a result, thermal effects on cells if there are any, are expected to be small. Zoom in: The sensing zone showing lines A, B, and C. (e) Simulated field along y-axis and a measured signal. It shows that the measured signal overlaps with simulated E-field energy density, as expected.

B. Microwave Spectroscopic Flow Cytometer

Fig. 1(a) is a schematic of the microwave flow cytometer used for *Candida* measurements. Its operation principle has been presented elsewhere [15]. Briefly, the tunable interferometer arrangement enhances signal-to-noise ratio (SNR) and enables convenient system recovery when environmental disturbances occur. Such recovery capability is important to obtain repeatable and reliable single cell measurement results for accurate cell property extraction and cell differentiation. Nevertheless, the

distribution of probing electric fields and cell location in the sensing zone also affect measurement repeatability and accuracy, which will be examined below. Additionally, cell size and shape, such as budding and nonbudding yeasts, are important cell parameters in cell analysis. Microscope-based imaging is added to the setup in Fig. 1(a).

The setup also facilitates convenient multiple frequency measurement, i.e., at the null frequency points in Fig. 1(b), and frequency tuning, i.e., by changing a cable length or adding a phase shifter in material-under-test (MUT) or Reference (Ref) branch in Fig. 1(a). Multifrequency measurement and tuning are necessary for dielectric spectroscopic studies of cells and desired for searching possible frequency points where the targeted cell species might have more distinctive dielectric properties.

The microstrip line (ML)-based sensing electrode in the MUT branch is shown in Fig. 1(c). A microfluidic channel (yellow) is integrated for yeast cell transport. A zoom-in of Fig. 1(c) shows a cross section of the ML. Fig. 1(d) and (e) show simulated vertical and horizontal distributions of probing microwave fields at a few different locations. The results show possible cell signal variations due to different cell transport trajectories. To minimize the variations, we only consider cells that pass over the ground plate, i.e., the yellow channel section in Fig. 1(c), in data process and analysis. For 4.5 μm diameter particles, the maximum estimated signal amplitude variation is 6% when the particle passes through the sensing zone at different vertical positions [15]. This variation will expand the distribution of intra-species cell properties and complicate microwave differentiation of cell types.

The microstrip line height h_{MUT} in Fig. 1(c) zoom-in determines measurement sensitivity. For h_{MUT} = 10 μm, *C. glabrata* cells (2-3 μm diameter) do not reliably produce high SNR microwave signals. Corresponding measurement data are not reported in this work. Moreover, the shape of the measured particle or cell signal in time domain should follow the horizontal field (i.e., energy) distribution in Fig. 1(e). When the carrier medium permittivity is determined through calibration, the cell induced effective permittivity change, $\Delta\varepsilon(f) = \Delta(\varepsilon'(f) - j\varepsilon''(f))$, can be quantified by use of the algorithms and formulas described in [15].

Fig. 2(a) shows typical measured yeast cell properties of the same viable *C. tropicalis* cell. The cell was manually handled to transport through the sensing zone more than once. The variation of the time-domain-signal width is due to nonuniform cell velocity. Nevertheless, the estimated $\Delta\varepsilon'$ and $\Delta\varepsilon''$ difference is only 0.07% and 0.68%, respectively. The small variations indicate good repeatability in manual cell handling of the same cell. The results also show high measurement accuracies. Fig. 2(b) and (c) show typical measured viable *C. tropicalis* cell signals when the cell passes the sensing zone at different x locations. Visually, cells 20 and 25 have similar sizes, and cell 20 is 2-3 μm away from the ground edge whereas cell 25 is close to the center of the microfluidic channel. Yet, the two *C. tropicalis* cells have 2.7% $\Delta\varepsilon'$ and 0.55% $\Delta\varepsilon''$ differences, which are much smaller than the estimated maximum variations for 4.5 μm particle discussed above. Thus, cell x location is unlikely to cause large signal variations. Nevertheless, more measurements would further help our understanding of measurement repeatability.

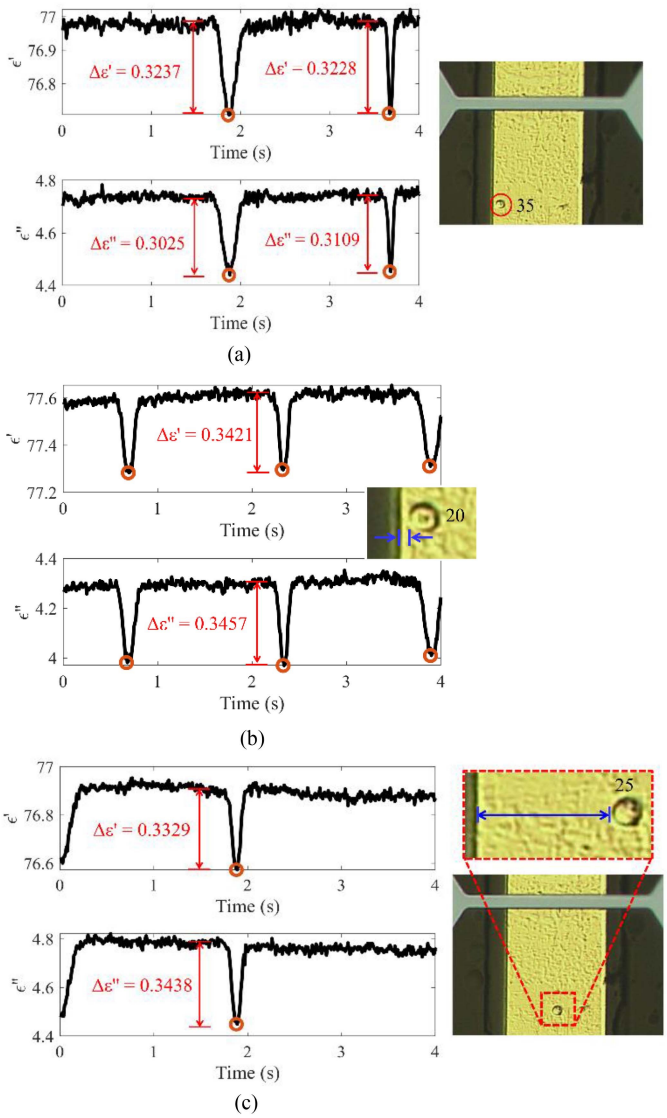

Fig. 2. Typical measured effective permittivity at f = 1.32 GHz for (a) a *C. tropicalis* cell passes through the sensing zone twice but at different speed, (b) a cell (estimated to be 7 μm in diameter) passes through the sensing zone at an *x*-location close to the ground edge (2-3 μm) three times, (c) a cell with similar size (≈ 7 μm) as the cell in (b) but at different location from the ground edge. $\Delta\varepsilon'$ and $\Delta\varepsilon''$ are cell induced permittivity changes.

III. Results and Discussions

A. Measurement Time Delay on Candida Microwave Properties

For each batch of yeast samples, a few hundred yeast cells were measured. Each measurement can take a few hours, during which yeast properties could have observable changes, thus, complicating microwave cell differentiation efforts. To determine if the time delay will affect microwave $\Delta\varepsilon(f)$, cultured yeast samples were divided into two parts. One part was characterized immediately while the other was stored for up to

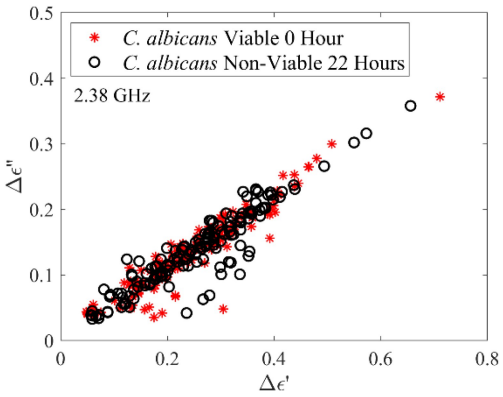

Fig. 3. The measured *C. albicans* microwave properties at 2.38 GHz.

24 hours at room temperature before microwave measurements. No noticeable changes to cell viability patterns were observed. This is consistent with the observations in [16]. Fig. 3 shows a comparison of typical microwave measurement results for *C. albicans*. Also, no obvious differences of cell $\varepsilon(f)$ distributions are observed. Thus, measured microwave property variations are unlikely due to delayed microwave measurements.

B. Candida Properties At Different Frequencies

Multiple frequency measurement of yeast samples was performed. The measurement frequencies were determined by arbitrarily chosen cable length differences (ΔL). No efforts were made to vary ΔL and cover more frequencies or to search for frequencies where interspecies $\Delta\varepsilon(f)$ are the best for cell differentiation. Furthermore, no sharp resonance features are expected, thus, minor null frequency point (Fig. 1(b)) drift with time is not expected to cause significant $\Delta\varepsilon(f)$ variation. So, frequency readings are rounded to 2- or 3-digit values after the decimal.

Two groups of measurements were conducted. The first group includes mixed budding and non-budding cells, but each cell was measured only at one frequency. Fig. 4(a) and (b) show the obtained $\Delta\varepsilon'(f)$ and $\Delta\varepsilon''(f)$. Wide intra-species variations (α_1, β_1) were observed. The intrinsic heterogeneity of cells was likely the main factor that cause the wide distributions. In the second group of measurement, each non-budding yeast cell was manually controlled for multiple frequency measurements. Typical results are shown in Fig. 4(c) and (d). More than a 50% reduction of the variations (α_2, β_2) and slightly smaller average $\Delta\varepsilon'(f)$ and $\Delta\varepsilon''(f)$, especially at higher frequencies was observed. These measurement changes were expected since budding cells can be twice the size of non-budding cells. Yet, the mean $\Delta\varepsilon'(f)$ and $\Delta\varepsilon''(f)$ for the two groups had different frequency-dependence. In Fig. 4(e) and (f), only a third of the cells from Fig. 4(c) and (d) are plotted. The overall permittivity distribution range (α_3, β_3) is only slightly reduced. Understandably, for each cell, its (α_3, β_3) across the measured frequencies was significantly smaller than (α_2, β_2). Surprisingly, the obtained $\Delta\varepsilon'(f)$ and $\Delta\varepsilon''(f)$ versus f in Fig. 4(e) and (f) lacked consistent trend or pattern. Nonrepeatable manual control could be a main factor

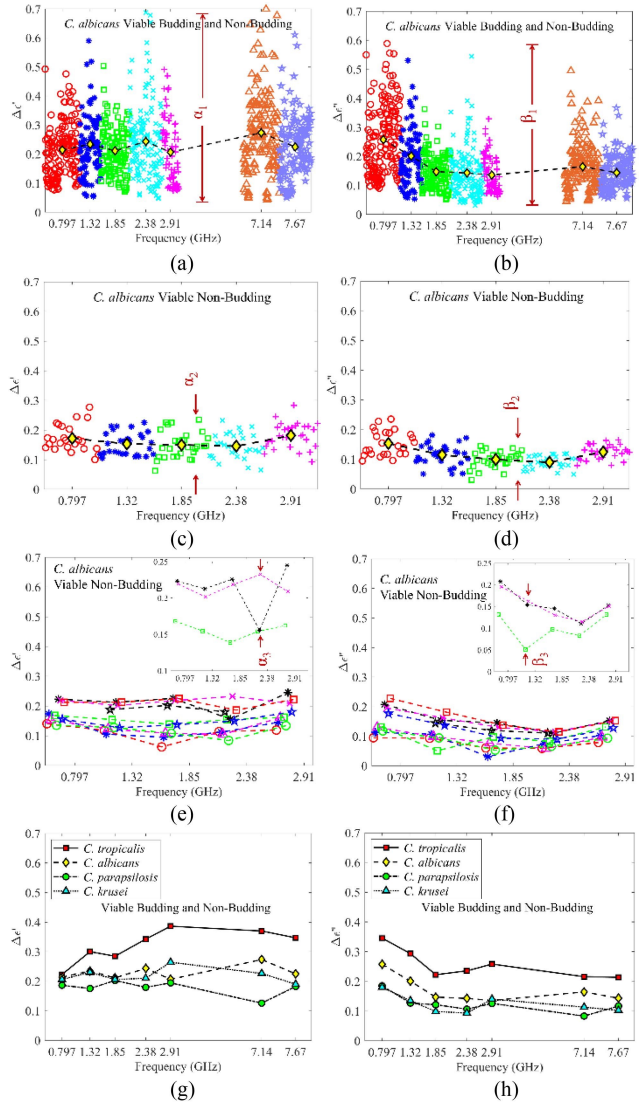

Fig. 4. (a) and (b) $\Delta\varepsilon'$ and $\Delta\varepsilon''$ of budding and non-budding *C. albicans* cell mixture, respectively. Each cell is measured at one frequency point. (c) and (d) $\Delta\varepsilon'$ and $\Delta\varepsilon''$ of non-budding *C. albicans* cells. The same cell is measured at all the frequency points. (e) and (f) Tracking the same non-budding cell through all the frequency points to determine any patterns. (g) and (h) Average of $\Delta\varepsilon'$ and $\Delta\varepsilon''$ of budding and non-budding *C. tropicalis*, *C. albicans*, *C. parapsilosis*, and *C. krusei*, each. Each cell is measured at one frequency point.

even though <1% difference in permittivity measurement is shown in Fig. 2(a) for the same *C. tropicalis* cell measured twice. The manual measurement of the same cell many times could cause the cell to travel along different flow lines or at different cell orientations during measurement, similar to that shown in Fig. 5(a) and (b). Thus, intrinsic frequency dependence of cell $\Delta\varepsilon(f)$ was overwhelmed by the uncontrolled fluctuations. Fig. 4(g) and (h) show the average $\Delta\varepsilon'(f)$ and $\Delta\varepsilon''(f)$ of the four *Candida* (viable). Different frequency relationship is observed. These differences imply potentially different molecular dynamics, i.e., the δ relaxation in [2], due to different molecular compositions between the species. At particular frequencies, such as 7.14 GHz, cell property differences were larger, which could be exploited for better cell differentiations. Nevertheless, more

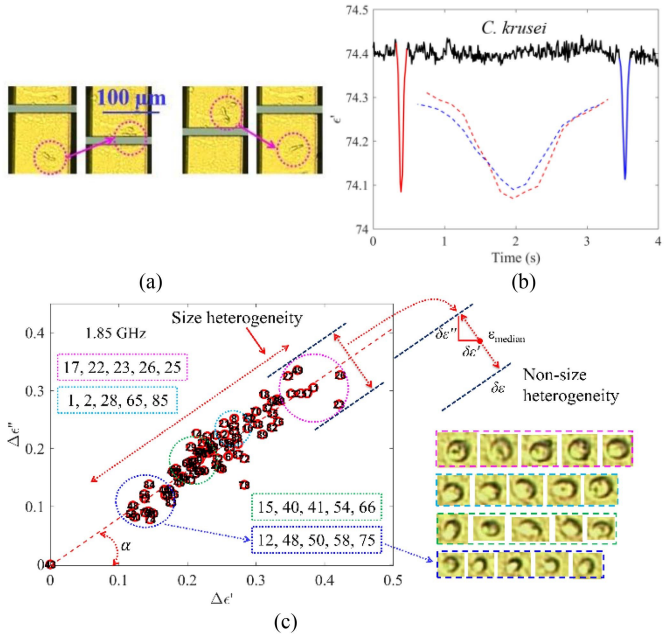

Fig. 5. (a) Budding *C. krusei* cell passing through the sensing zone at different orientations, (b) Signals produced by the same budding *C. krusei* cell at 1.85 GHz when the cell passes through the sensing electrode at different orientations. The inset overlays of the two signals and shows that the peak signal levels depend on cell orientation. (c) Intra-species permittivity variation of *C. tropicalis* cells. It shows that size heterogeneity is dominant.

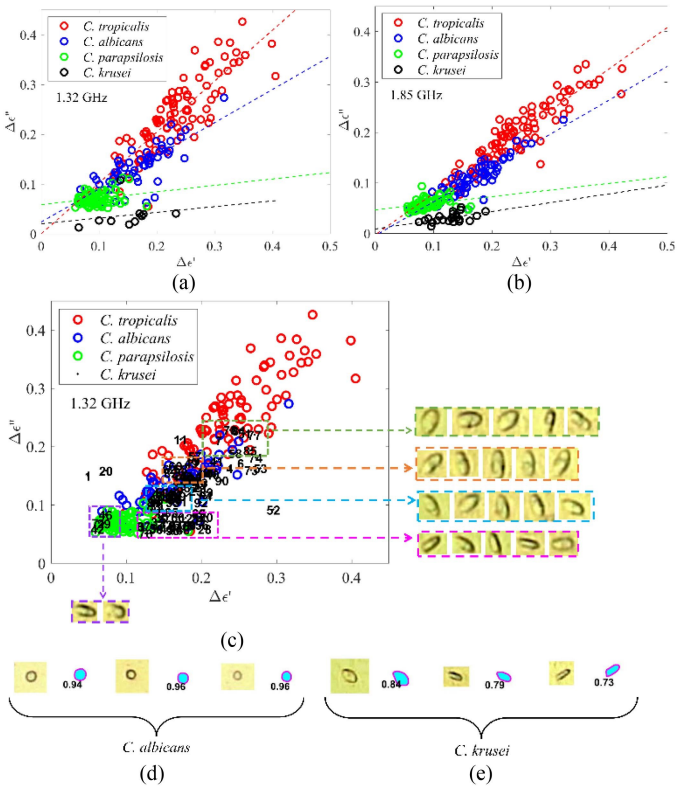

Fig. 6. (a) and (b) Measured $\Delta\varepsilon'(f)$ versus $\Delta\varepsilon''(f)$ of non-budding *C. tropicalis*, *C. albicans, C. parapsilosis*, and *C. krusei* at 1.32 GHz and 1.85 GHz, respectively. Non-budding *C. krusei* is manually picked from cell mixture measurement containing budding and non-budding cells. (c) Cell properties overlap due to budding *C. krusei* cells at 1.32 GHz. (d) and (e) Optical images used to aid cell shape differentiation, *C. albicans* cells (round shape) and *C. krusei* cells (oval-oblong shape).

cell and environmental factor effects need to be investigated, in conjunction with biochemical analysis, to further examine and verify the observations.

C. Microwave Characterization of Cell Heterogeneity

Fig. 4 shows that *Candida* have wide property distributions, i.e., significant heterogeneity. The cell size difference is an obvious type of heterogeneity, e.g., larger (α_1, β_1) for budding cells in Fig. 4(a)-(b) than smaller (α_2, β_2) for non-budding cells in Fig. 4(c)-(d). The cell shape difference is another factor, as shown in the MHz frequencies [3], [4]. In addition, signals from nonspherical budding cells depend on cell orientations during measurement. Fig. 5(a) shows two pictures of the same budding cell for two consecutive measurements. Fig. 5(b) shows corresponding microwave signals, which have significantly different shape and amplitude. The signal amplitude ($\Delta\varepsilon$ in Fig. 2) was used for analysis in Fig. 4. Thus, such non-intrinsic factors, which are difficult to remove from the current data, also contribute to the observed variations. Additional measurements, such as those exploited in [5], are needed for cell budding and measurement orientation determination.

After visually removing budding cells, Fig. 5(c) shows that $\Delta\varepsilon'$ and $\Delta\varepsilon''$ for *C. tropicalis* are more consistent. Fig. 5(c) also shows the microscopic images for selected cells, which were labeled. Larger *C. tropicalis* cells exhibit higher $\Delta\varepsilon'$ and $\Delta\varepsilon''$ at 1.85 GHz, and at other frequencies (not shown). Furthermore, the average $\Delta\varepsilon'$ vs $\Delta\varepsilon''$ exhibit a colinear dependence, i.e., a straight line that passes the origin (00) at an angle α when cell size changes. The line is close to the least-square (LS) fitting line, hereafter described as LS line. The colinear relationship implies the molecular composition profile of *C. tropicalis* remains the same for cells of different sizes. Such conservations are the foundation of mass spectroscopy for cell identifications [6]. Thus, this component of heterogeneity can be separated from non-size heterogeneity components, as illustrated in Fig. 5(c). It shows that ($\delta\varepsilon'$, $\delta\varepsilon''$) is likely a conservative estimation of non-size cell intrinsic heterogeneity and it is much smaller than cell size heterogeneity. Assume the cells in the magenta circle have the same size with an average $\Delta\varepsilon_{median}$ ($\Delta\varepsilon_a'$, $\Delta\varepsilon_a''$). The estimated $\delta\varepsilon/\Delta\varepsilon$ is approximately 9%, which is comparable with the measurement accuracy of the flow cytometer.

D. Candida Microwave Properties For Cell Species Classification

Fig. 6(a) and (b) show the measured $\Delta\varepsilon(f)$ of single non-budding *C. albicans*, *C. tropicalis*, *C. parapsilosis,* and *C. krusei* at 1.32 GHz and 1.85 GHz, respectively. Quadratic discriminate analysis (QDA) shows that the specificity is at least 0.87 at both the frequencies. This signal separation will enable potential classification of yeast species. These profiles show that the size related LS lines have different slopes, which imply different

molecular compositions of different cell species. Similar results are obtained at other frequencies, but with different line slopes, i.e., different molecular dynamics properties, similar to the observations in Fig. 5. The LS line for *C. parapsilosis* (CP) does not pass through the origin, which indicates strong non-size heterogeneity though further work is needed to deter-mine the mechanisms. Nevertheless, the LS line slope α and its frequency dependence can be further explored for microwave spectroscopic cell discrimination.

Without visual selection of non-budding *C. krusei* cells, the $\Delta\varepsilon'(f)$ vs $\Delta\varepsilon''(f)$ distributions have severe overlaps, as shown in Fig. 6(c). Detailed microscopy image examination in Fig. 6(c) shows *C. krusei* is mostly budding, which exacerbates the spreading and overlapping issues as discussed for Fig. 6(a) and (b). Moreover, budding *C. krusei* cells seem to have a different LS line slope or multi-section LS line. As discussed above, shape induced dispersion [4], [7] and cell orientation during measurement are some other factors that need to be identified.

Optical imaging can be combined with microwave measurement to better discriminate *Candida* species, such as *C. albicans* and *C. krusei* shown in Fig. 6(d) and (e). For each *C. albicans* and *C. krusei* cell, the original cell image is on the left, and the image processed by MATLAB Image Processing Toolbox is on the right. The number displayed next to the processed image is calculated by MATLAB, and it is equal to $4\pi A/P^2$ where A is the area, and P is perimeter of the image. The closer to 1 this number is, the more circular the image is. All the *C. albicans* images return a number > 0.92 whereas all the *C. krusei* images return a number < 0.85.

E. Candida Viability and Drug Effect

Non-viable *Candida* that had been heat shocked were measured at several frequencies from 0.796 GHz to 7.67 GHz. Fig. 7 shows some typical results. Fig. 7(a) shows clear microwave property separations between viable and non-viable cells, regardless of budding status. The slight overlap between viable and non-viable cells towards the origin point of Fig. 7(a) is likely caused by a few viable cells in the non-viable samples and non-viable cells in the viable samples. Testing showed that heat-shocked cells did not exclude trypan blue, which indicated leaky cell wall/membrane. Thus, heat-shocked *Candida* will exchange cell cytoplasm with diluted culture medium. As a result, $\Delta\varepsilon''(f)$ is close to that of the medium, i.e., with smaller $\Delta\varepsilon''(f)$ than viable cells. When frequency increases, the difference between viable and non-viable cells is reduced as shown in Fig. 7(b) to (d). Yet, slight differences are still seen at 7.67 GHz. However, the small difference indicates possible molecular composition changes of each *Candida* species. Similar $\Delta\varepsilon'(f)$ vs $\Delta\varepsilon''(f)$ trends are observed for other *Candida* species.

Caspofungin (CSP) diacetate in dimethly sulfoxide (DMSO) was used to investigate the microwave signal changes due to a drug effect. Drugs of different doses were used to treat 10^6 cells in 1 mL. Microwave measurements started 10 minutes after drug application. It took 30–60 minutes to examine 40–60 cells. For CSP, the limited measurement time duration was expected to not cause significant issues as the 24-hour reading

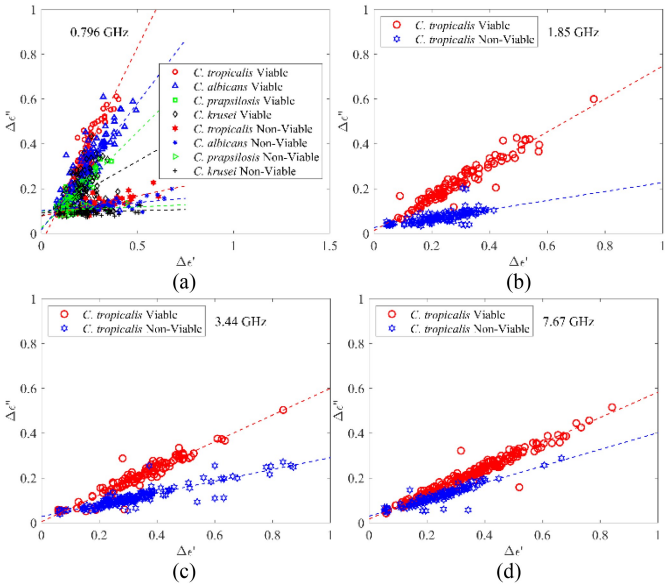

Fig. 7. (a) Measured permittivity values of viable and non-viable *Candida* at 0.796 GHz. (b) to (d) Measured permittivity values of viable and non-viable *C. tropicalis* at 1.85 GHz, 3.44 GHz, and 7.67 GHz, respectively.

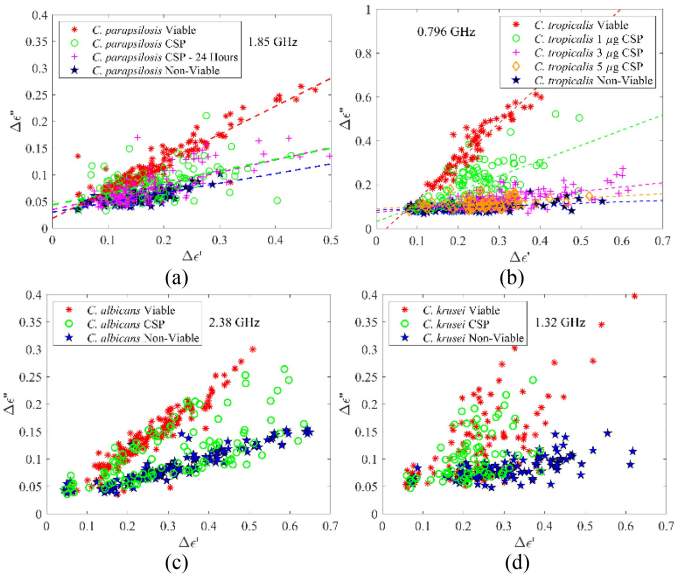

Fig. 8. Microwave measurement of *Candida* species exposed to CSP at different frequencies. (a) *C. parapsilosis*, (b) *C. tropicalis*, (c) *C. albicans*, and (d) *C. krusei*.

delay for *C. parapsilosis* produced similar scatter profiles. Drug concentration that causes 50% cell death, such as CSP shown in Fig. 8(b), is considered the drug minimum inhibitory concentration (MIC). Changing drug concentration and measuring the shifts of microwave responses, Fig. 8(c) and (d) show the responses of *C. albicans* and *C. krusei* to CSP at an estimated CSP MIC.

The microwave determined MIC was significantly higher than the MIC values obtained when cells are cultured for 24–48 hours on agar plates inoculated at low cell concentrations. Temperature

is one of the factors that potentially contributed to the discrepancies since the microwave measurements are performed at 20 °C (room temperature) while culture methods use 32 °C to 37 °C. Further work is needed to better understand the microwave MIC and its relationship with culture-based methods.

The above measurement results include effects of many other factors not yet discussed, such as measurement temperature changes, cell cycles, cell motion (mechanical forces), measurement system errors, and non-repeatable measurement operations. The effects reduce the accuracy of the obtained property values of each cell and widen the distribution of permittivity scatter plots. However, with sufficient number of measured cells, the population average of each cell type is accurate.

Compared with other microwave single-cell measurement techniques, such as coplanar waveguide (CPW) based broadband methods with mechanical cell blocker [24] or shunt configuration [25], microwave interferometer and resonator based dielectrophoresis spectroscopy (beta-dispersion measurement) [26], integrated circuit based multi-frequency platform which measures GHz cell opacity values, this work does not trap cells and provides quantitative $\Delta\varepsilon'(f)$ and $\Delta\varepsilon''(f)$ of single cells. Therefore, it is an effective approach to analyze cells in native state, including examining cell heterogeneity, species, viability and drug effects. Non-budding *Candida* of the same species or viability have similar molecular composition profiles, as the microwave properties, $\Delta\varepsilon_a'(f)$ and $\Delta\varepsilon_a''(f)$, follow colinear relationships. Different species have different colinear coefficients (i.e., α values in Fig. 5(c)), which are likely due to different molecular compositions. Viable and non-viable cells of the same species also have different colinear coefficients. Furthermore, the α values are frequency dependent, which indicate different molecular dynamics properties. Thus, broadband and quantitative measurements of single *Candida* cell are promising for discriminating cell species, similar to mass-spectroscopy for yeast and bacteria identification.

Future work is needed for improved cell discrimination. For example, a simultaneous measurement of cell volume and budding, non-budding state should be included to address some of the microwave property overlap issues. Accurate measure-ment of the same cell at different frequencies over a wide frequency range without the manual operation may reveal more cell dynamic characteristics that are specific to cell species and or physiological states. Beyond *Candida*, characterizing other cell types, such as immune cells (i.e., white blood cells), and cell states, such as rest or activated (by *Candida*) immune cells, is of great interest and importance. Furthermore, efforts are needed to achieve high throughput and low-cost operation. Corresponding limiting factors are the VNA in Fig. 1(a) and sample preprocessing methods. Lastly, significant differences of *Candida* responses to different antifungal drugs may help improve *Candida* species identification. This potential is unique to the described microwave technique since *Candida* are intact after measurement. Ultimately, what physicians need is information to select a drug and dose to treat a candidemia patient, regardless of the yeast species. Therefore, microwave techniques are a promising tool for rapid candidemia diagnosis.

IV. Conclusion

A simple microwave flow cytometer, based on a vector network analyzer and an interferometer, is shown for effective measurement of single *Candida* cells at different frequencies between 0.265 GHz and 7.67 GHz. Quantitative permittivity values, $\Delta\varepsilon'(f)$ and $\Delta\varepsilon''(f)$, enable cell heterogeneity analysis, despite relatively large measurement variations. These results show that cell $\Delta\varepsilon'(f)$ and $\Delta\varepsilon''(f)$ are colinear with cell volumes, and cells of different species and viability states have different colinear coefficients. The coefficients are also frequency dependent. These observations imply that the molecular compositions of the same *Candida* species are conserved. These characteristics will enable microwave cell identification. However, the budding status and cell orientation during measurement affect $\Delta\varepsilon'(f)$ and $\Delta\varepsilon''(f)$.

Viable and heat-shocked non-viable yeast cells have significantly different permittivity values at lower frequencies, which allows for a straightforward cell viability determination. At higher frequencies, such as 7.67 GHz, the differences are small probably due to diminished effects of cytoplasm conductivity. Single, non-budding *Candida* cells of different species have significantly different $\Delta\varepsilon(f)$, with a minimum specificity of 0.87. New approaches for simultaneous measurement of cell volume, shape, and microwave property at multiple frequencies are needed for better specificity. The microwave measurement of *Candida* exposed to CSP demonstrated that a microwave method could potentially provide a real-time technique for antifungal susceptibility test. Further work is needed to better understand the relationship between the MICs of single cell microwave measurement and cell culture method. Most promising is the capability of the microwave assessment of *Candida* species to aid discrimination of drug therapies for effective candidemia treatment. Thus, broadband microwave measurements hold much potential as a new approach for accurate candidemia diagnosis, and assessment of drug candidates for treatment.

References

[1] H. Wisplinghoff, T. Bischoff, S. M. Tallent, H. Seifert, R. P. Wenzel, and M. B. Edmond, "Nosocomial bloodstream infections in US hospitals: Analysis of 24,179 cases from a prospective nationwide surveillance study," *Clin. Infect. Dis.*, vol. 39, no. 3, pp. 309–317, 2004.

[2] M. Toda et al., "Population-based active surveillance for culture-confirmed candidemia—Four sites, United States, 2012–2016," *MMWR Surveill. Summ.*, vol. 68, no. 8, 2019, Art. no. 1.

[3] S. Strollo, M. S. Lionakis, J. Adjemian, C. A. Steiner, and D. R. Prevots, "Epidemiology of hospitalizations associated with invasive candidiasis, United States, 2002–2012," *Emerg. Infect. Dis.*, vol. 23, no. 1, 2017, Art. no. 7.

[4] M. Morrell, V. J. Fraser, and M. H. Kollef, "Delaying the empiric treatment of Candida bloodstream infection until positive blood culture results are obtained: A potential risk factor for hospital mortality," *Antimicrob. Agents Chemother.*, vol. 49, no. 9, pp. 3640–3645, 2005.

[5] P. G. Pappas, M. S. Lionakis, M. C. Arendrup, L. Ostrosky-Zeichner, and B. J. Kullberg, "Invasive candidiasis," *Nat. Rev. Dis. Primers*, vol. 4, no. 1, pp. 1–20, 2018.

[6] C. Zurl et al., "T2Candida magnetic resonance in patients with invasive candidiasis: Strengths and limitations," *Med. Mycol.*, vol. 58, pp. 632–638, 2020.

[7] Center for disease control and Prevention, "Invasive candidiasis statistics," 2021. [Online]. Available: https://www.cdc.gov/fungal/index.html

[8] M. Safavieh et al., "Advances in Candida detection platforms for clin-ical and point-of-care applications," *Cr. Rev. Biotechn.*, vol. 37, no. 4, pp. 441–458, 2017.
[9] D. Holmes et al., "Leukocyte analysis and differentiation using high speed microfluidic single cell impedance cytometry," *Lab Chip*, vol. 9, no. 20, pp. 2881–2889, 2009.
[10] F. Artis et al., "Microwaving biological cells: Intracellular analysis with microwave dielectric spectroscopy," *IEEE Microw. Mag.*, vol. 16, no. 4, pp. 87–96, May 2015.
[11] A. Di Biasio and C. Cametti, "Effect of shape on the dielectric proper-ties of biological cell suspensions," *Bioelectrochemistry*, vol. 71, no. 2, pp. 149–156, 2007.
[12] K. Asami, "Dielectric dispersion in biological cells of complex geometry simulated by the three-dimensional finite difference method," *J. Phys. D: Appl. Phys.*, vol. 39, no. 3, 2006, Art. no. 492.
[13] M. Shaker, L. Colella, F. Caselli, P. Bisegna, and P. Renaud, "An impedance-based flow microcytometer for single cell morphology discrimination," *Lab Chip*, vol. 14, no. 14, pp. 2548–2555, 2014.
[14] C. V. Bertelsen, J. C. Franco, G. E. Skands, M. Dimaki, and W. E. Svendsen, "Investigating the use of impedance flow cytometry for classifying the viability state of E. coli," *Sens.*, vol. 20, no. 21, 2020, Art. no. 6339.
[15] J. A. Osterberg et al., "Microwave sensing of yeast cell species and viability," *IEEE Trans. Microw. Theory Techn.*, vol. 69, no. 3, pp. 1875–1886, Mar. 2021.
[16] Public Health Agency of Canada, "Pathogen safety data sheets: Infectious substances – Candida albicans," 2021. [Online]. Available: https://www.Canada.ca/en/public-health/services/laboratory-biosafety-biosecurity/pathogen-safety-data-sheets-risk-assessment.html
[17] X. Xie et al., "Particle self-aligning, focusing, and electric impedance microcytometer device for label-free single cell morphology discrimination and yeast budding analysis," *Anal. Chem.*, vol. 91, no. 21, pp. 13398–13406, 2019.
[18] C. V. Weis, C. R. Jutzeler, and K. Borgwardt, "Machine learning for microbial identification and antimicrobial susceptibility testing on MALDI-TOF mass spectra: A systematic review," *Clin. Microbiol. Infec.*, vol. 26, pp. 1310–1317, 2020.
[19] M. Pfaller, L. Boyken, R. Hollis, S. Messer, S. Tendolkar, and D. Diekema, "In vitro susceptibilities of Candida spp. to caspofungin: Four years of global surveillance," *J. Clin. Microbiol.*, vol. 44, no. 3, pp. 760–763, 2006.
[20] S. Gil-Alonso, N. Jauregizar, E. Eraso, and G. Quindós, "Postantifungal effect of caspofungin against the Candida albicans and Candida parapsilosis clades," *Diagn. Microbiol. Infect. Dis.*, vol. 86, no. 2, pp. 172–177, 2016.
[21] S. Gil-Alonso, N. Jauregizar, E. Cantón, E. Eraso, and G. Quindós, "In vitro fungicidal activities of anidulafungin, caspofungin, and micafungin against Candida glabrata, Candida bracarensis, and Candida nivariensis evaluated by time-kill studies," *Antimicrob. Agents Chemother.*, vol. 59, no. 6, pp. 3615–3618, 2015.
[22] N. Heintz and S. Gong, "Small-Scale preparations of yeast DNA," *Cold Spring Harb Protoc*, vol. 10, pp. 430–432, 2020.
[23] X. Xu, H. Lv, F. Zhang, H. Zhu, and L. Cai, "A comparison of Candida detection in sputum by the conventional culture and fluorescent polymerase chain reaction methods," *Med. Sci. Monit.*, vol. 27, 2021, Art. no. e930293.
[24] A. Tamra, D. Dubuc, M. -P. Rols, and K. Gernier, "Microwave monitor-ing of single cell monocytes subjected to electroporation," *IEEE Trans. Microw. Theory Techn.*, vol. 65, no. 9, pp. 3512–3518, Sep. 2017.
[25] X. Ma, X. Du, H. Li, X. Cheng, and J. C. M. Hwang, "Ultra-Wideband impedance spectroscopy of a live biological cell," *IEEE Trans. Microw. Theory Techn.*, vol. 66, no. 8, pp. 3690–3696, Aug. 2018.
[26] S. Afshar et al., "Full beta-dispersion region dielectric spectra and dielectric models of viable and non-viable CHO cells," *IEEE J. Electromagn. RF Microw. Med. Biol.*, vol. 5, no. 1, pp. 70–77, Mar. 2021.
[27] J. Chien et alet al., "A high-throughput flow cytometry-on-a-CMOS platform for single-cell dielectric spectroscopy at microwave frequencies," *Lab Chip*, vol. 18, pp. 2065–2076, 2018.